The tropical route of QBO teleconnections in a climate model

Jorge L. García-Franco[1], Lesley J. Gray[1,2], Scott Osprey[1,2], Robin Chadwick[3,4], and Zane Martin[5]

[1]Atmospheric, Oceanic and Planetary Physics, University of Oxford, Oxford, UK
[2]National Centre for Atmospheric Science, UK
[3]Met Office Hadley Centre, Exeter, UK
[4]Global Systems Institute, Department of Mathematics, University of Exeter, Exeter, UK
[5]Department of Atmospheric Science, Colorado State University, Fort Collins, CO

Correspondence: Jorge L. García-Franco (jorge.garcia-franco@physics.ox.ac.uk)

Abstract. The influence of the quasi-biennial oscillation (QBO) on tropical climate is demonstrated using a 500-yr pre-industrial control simulation of the Met Office Hadley Centre model. Robust precipitation responses to the phase of the QBO are diagnosed in the model which show zonally asymmetric features, consistent with observational studies. The response in precipitation resembles the El Niño-Southern Oscillation (ENSO) impacts, however, regression analysis shows that there is a QBO signal in precipitation that is independent from ENSO. Moreover, the observed uneven frequency of ENSO events for each QBO phase is also found in these simulations, with more El Niño events found under the westerly phase of the QBO (QBOW) and more La Niña events for the easterly phase (QBOE). No evidence is found to suggest that these QBO-ENSO relationships are caused by ENSO modulating the QBO in the simulations. A previously unknown relationship between the QBO and a dipole of precipitation in the Indian Ocean is found in models and observations in boreal fall, characterized by a wetter western Indian Ocean and drier conditions in the eastern part for QBOW and the opposite under QBOE conditions. QBO W-E differences show a stronger East Pacific Inter-tropical Convergence Zone (ITCZ) in boreal winter and a northward shift of the Atlantic ITCZ in boreal spring and summer. The Walker circulation is found to be significantly weaker during QBOW compared to QBOE, explaining the observed and simulated zonally asymmetric responses at equatorial latitudes. Further work, including targeted model experiments, is required to betters understand the mechanisms causing these relationships between the QBO and tropical convection.

1 Introduction

Long-distance effects or teleconnections associated with the stratospheric quasi-biennial oscillation (QBO) have been well documented in the subtropics and extratropics, including for example: the stratospheric polar vortex (Holton and Tan, 1980; Anstey and Shepherd, 2014; Lu et al., 2020), the subtropical jets (Garfinkel and Hartmann, 2011b; Hansen et al., 2016; Ma et al., 2021) and the North Atlantic Oscillation (Hansen et al., 2016; Gray et al., 2018; Andrews et al., 2019b). Observational and modelling evidence suggests that there is also a tropical route of influence of the QBO through impacts on: monsoons (Giorgetta et al., 1999; Claud and Terray, 2007; Liess and Geller, 2012), the Intertropical Convergence Zone (ITCZ) (Gray et al., 2018), tropical sea-surface temperatures (SSTs) (Garfinkel and Hartmann, 2011a; Huang et al., 2012) and convective

clouds (Liess and Geller, 2012; Peña-Ortiz et al., 2019), tropical cyclones (Ho et al., 2009; Jaramillo et al., 2021), and most
25   prominently, the Madden-Julian Oscillation (MJO) (Son et al., 2017; Lee and Klingaman, 2018; Wang et al., 2019; Martin
et al., 2021b). For recent reviews on stratosphere-troposphere coupling in the tropics, see Haynes et al. (2021) and Hitchman
et al. (2021).

The tropical route of QBO teleconnections remains less well understood than other routes for various reasons. The short
observational record limits the confidence in any analysis that seeks to investigate differences between the two QBO phases
30   in a 30-40-yr long dataset, as variability in the tropics on QBO time-scales is dominated by El Niño-Southern Oscillation
(ENSO) (Liess and Geller, 2012; Seo et al., 2013; Gray et al., 2018). Similarly, the modulation of the location and magnitude
of convection in the tropical Pacific by ENSO events can influence the characteristics of the QBO (Taguchi, 2010; Schirber,
2015; Christiansen et al., 2016; Serva et al., 2020), which makes it difficult to separate the cause and effects of ENSO and the
QBO.
35   The physical mechanisms through which the QBO could influence tropical climate are also not well understood. The influ-
ence of the QBO over the temperature and vertical wind shear near the tropopause layer (Tegtmeier et al., 2020; Martin et al.,
2021c) has been hypothesized to affect convection through several mechanisms. Early studies (Gray, 1984; Collimore et al.,
2003) suggest that changes to the vertical wind shear or static stability in the upper-troposphere lower-stratosphere (UTLS)
region induced by the QBO modify the depth of convection at equatorial latitudes. However, other studies suggest that the
40   surface impact of the QBO may be a function of both the UTLS temperature changes and the tropospheric convective forcing
(Nie and Sobel, 2015).

However, multiple lines of evidence suggest that there is a modulation of several features of tropical climate by the QBO.
In observations, surface impacts of the QBO over monsoon regions have been diagnosed in satellite-derived fields such as
cloud height, occurrence and out-going longwave radiation (Collimore et al., 2003; Liess and Geller, 2012), as well as in
45   surface precipitation diagnosed from gridded datasets or from reanalysis (Seo et al., 2013; Gray et al., 2018). However the
observational evidence shows zonally asymmetric impacts – indicating that the QBO influence depends on longitude. The
proposed mechanism is linked to a QBO modulation of the Walker circulation (e.g. by Collimore et al., 2003; Liess and Geller,
2012), which appears in some reanalysis (Hitchman et al., 2021).

In model studies, Giorgetta et al. (1999) found that boreal summer monsoon regions exhibit a significant response in cloudi-
50   ness to the QBO winds in a General Circulation Model (GCM). In a cloud-resolving model, Nie and Sobel (2015) found that
the influence of the QBO may depend on the strength of convection and SST forcing, suggesting a non-linear effect of the QBO
over a convective profile. Analyses of seasonal and sub-seasonal forecast models have focused on the QBO-MJO relationship
(Lim et al., 2019; Klotzbach et al., 2019; Martin et al., 2020) finding that the MJO is stronger and more predictable under
the easterly phase in the lower stratosphere. However, only a relatively small number of studies have analysed tropical QBO
55   teleconnections in CMIP5/CMIP6 models (Serva et al., submitted), as most CMIP analyses focus on the overall representation
of the QBO and teleconnections to the extra-tropics (Richter et al., 2020; Anstey et al., 2021), whereas Kim et al. (2020) found
that the CMIP6 models do not reproduce the observed MJO-QBO relationship.

It remains unclear whether the QBO has any effect on convection at the local-scale or through the large-scale tropical circu-lation. Moreover, in the short observational record, ENSO is a strong confounding influence, which means long integrations of

60 GCMs could provide better statistics and understanding of the surface impact of the QBO in the tropics. This paper investigates the tropical route of QBO influence using simulations of the UK Met Office Hadley Centre (MOHC) Unified Model submitted to the Climate Model Intercomparison Project CMIP6. The model extends to the mesosphere and includes a self-generated QBO via a non-orographic gravity wave scheme that compares well with the observed QBO (Richter et al., 2020).

The CMIP6 pre-industrial control (piControl) experiments with constant 1850 external forcing are examined to exploit their

65 length (500-yr) and the resulting statistical robustness of the diagnosed QBO impacts. The main purpose of this investigation is to diagnose whether there are any robust impacts in the tropical troposphere within a long integration of a state-of-the-art GCM. The focus of this study are the large-scale QBO impacts within the tropical troposphere. QBO-MJO connections are excluded from this study as they have already been explored and found largely absent the the MOHC models (Kim et al., 2020).

The paper is structured as follows. Section 2 describes the simulations together with the observational and reanalysis data

70 that are employed for comparison and verification, as well as the composite and regression techniques employed in the study. Section 3 examines evidence for QBO signals in a variety of tropical climate indicators, including precipitation, the ITCZ, monsoons, ENSO, the Walker circulation and the Indian Ocean Dipole (IOD). The final section provides a summary and conclusions of the main findings.

2 Methods and data

2.1 Observations and reanalysis

75 The gridded precipitation datasets used in this study are the $1°$ resolution Global Precipitation Climatology Project (GPCP) v2.3 (Adler et al., 2003) dataset and the Global Precipitation Climatology Centre (GPCC) dataset version 6 (Becker et al., 2011; Schneider et al., 2011). GPCP is a merged product of satellite and land rain-gauge observations and provides coverage over land and ocean, whereas GPCC uses a large network of surface station data and has a higher horizontal resolution but

80 does not provide data over oceanic regions (Becker et al., 2013; Adler et al., 2018).

For the other diagnostics, including zonal wind, vertical velocity and convective precipitation, we use the European Centre for Medium-Range Weather Forecasts (ECMWF) ERA5 Reanalyses (Hersbach et al., 2020) downloaded at the $0.75°x0.75°$ resolution from https://cds.climate.copernicus.eu/cdsapp. Gridded SSTs are obtained from the HadSST v3 (Kennedy et al., 2011). For observations and ERA5 datasets all available data spanning the period 1979-2018 are used. Note that for GPCC the

85 period covered is 1979-2014.

2.2 CMIP6 data

CMIP6 piControl simulations from two versions of the coupled ocean-atmosphere MOHC Unified Model are examined. The HadGEM3 model is the core physical climate model and UKESM1 is an Earth System Model extension, with additional

treatment of aspects of e.g. land surface, ocean and sea ice processes as well as improved chemical processes (Kuhlbrodt
90 et al., 2018; Williams et al., 2018; Sellar et al., 2019). Three piControl experiments are analysed: HadGEM3 GC3.1 at N96
and N216 horizontal resolutions (hereafter referred to as GC3 N96-pi and GC3 N216-pi) and UKESM at N96 horizontal
resolution (hereafter referred to as UKESM N96-pi). The N96 and N216 atmospheric resolution is $1.875°$x$1.25°$ and $0.83°$x
$0.56°$, respectively whereas their oceanic resolutions are $1°$ (ORCA1) and $0.25°$ (ORCA025), respectively.

The full 500 years available for the GC3 N216-pi simulation are used and although more data exists for UKESM-pi and GC3
95 N96-pi, we use 500-yrs of these simulations for statistical consistency. These data are publicly available without registration
at the Earth System Grid Federation (ESGF) portal of CEDA: https://esgf-index1.ceda.ac.uk/search/cmip6-ceda/. The three
simulations have the same experimental design with constant year-1850 external forcing, further detail about the MOHC
piControl experiments can be found in Menary et al. (2018) and about the UKESM1 model in Sellar et al. (2019).

The majority of diagnostics are shown for the higher resolution GC3 N216-pi simulation and comparisons with the other
100 two simulations are noted where appropriate. The equatorial climate of GC3 N216-pi captures tropical dynamical processes
and tropical mean and extreme precipitation reasonably well relative to lower-resolution configurations (García-Franco et al.,
2020; Abdelmoaty et al., 2021). This configuration has been compared with other CMIP5/CMIP6 models in metrics such as the
seasonal-phase locking and amplitude of ENSO (Menary et al., 2018; Richter and Tokinaga, 2020; Liu et al., 2021), extreme
precipitation (Abdelmoaty et al., 2021) and the annual cycle of equatorial Atlantic SSTs and low-level winds (Richter and
105 Tokinaga, 2020). Furthermore, this and previous versions of the HadGEM model have well represented the stratosphere and
the QBO (Schenzinger et al., 2017; Richter et al., 2020). However, several biases are notable in this model, particularly in
tropospheric dynamical features such as the southward bias of the Atlantic ITCZ linked to the dry Amazon bias and overly
strong precipitation rates over the East Pacific ITCZ (García-Franco et al., 2020).

2.3 Indices

110 The QBO is characterised using ERA5 monthly-mean zonal-mean zonal winds at 70 hPa averaged between $5°$S-$5°$N. The
QBO phase is defined using a threshold of 2 m s^{-1} (Garfinkel and Hartmann, 2010), so the transition years where the QBO
winds fall within the range $\pm$ 2 m s^{-1} are excluded. The EN3.4 SST index is used to characterise ENSO by area-averaging the
box within $5°$S-$5°$N and $190°$E-$240°$E. A 5-month running-mean of the index is calculated and a threshold of ±0.5 K used to
define positive (El Nino) or negative (La Nina) events. Neutral months are defined where the magnitude of the EN3.4 index is
115 smaller than ±0.5 K.

The amplitude and descent rates of the QBO are calculated using the deseasonalized zonal mean zonal wind averaged over
the stated latitudes for all levels. The amplitude (A) of the QBO is defined using the first and second principal components
(PCs) following an empirical orthogonal function (EOF) decomposition of the 10-70 hPa wind time-series (Serva et al., 2020)
as $A = \sqrt{PC1^2 + PC2^2}$. The descent rates are calculated following Schenzinger et al. (2017) for descending westerly and
120 easterly phases individually by finding the level of the zero wind line ($u = 0$) for each month and computing the difference
between consecutive months. These definitions of the amplitude and descent rates were chosen to evaluate the influence of
ENSO on the whole profile of the QBO and not just one single level.

For the Indian Ocean Dipole (IOD), a convective precipitation index of the zonal gradient in the Indian Ocean (convective IOD Index) was defined as the difference of the deseasonalized area-averaged convective precipitation between the western

125 [50-70°E] and eastern [80-100°E] equatorial [10°S-10°N] Indian Ocean, which is in a similar region as the standard SST IOD index (Wang and Wang, 2014). This convective precipitation index is used to define IOD events with a 1 standard deviation threshold to define positive and negative events.

2.4 Analysis techniques

Composite analysis is the primary technique used in the study. For each month the QBO phase (QBO-E or QBO-W) and the

130 ENSO phase (El Niño, La Niña or neutral ENSO phase) was determined as described above. Annual-mean and seasonal-mean composites were derived by computing weighted averages to account for differences in the counts of each month and avoid a possible seasonal effect due to, e.g., QBO or ENSO phase-locking (see appendix A1).

The length of the experiments is such that the number of total El Niño and La Niña months for GC3 N216-pi were over 1500 months in the entire simulation for each phase, and over 2300 months for each QBO phase. Moreover, El Niño months found

135 under QBOW were 376 and 284 under QBOE, whereas in the observed 1979-2018 period, 62 QBOW El Niño months and 36 QBOE El Niño months were diagnosed.

Linear regression analysis is also employed to explore the impact of one or more of the indices, as in previous studies that examined QBO impacts at the surface (Gray et al., 2018; Misios et al., 2019). Details of the regression analysis technique are provided in the appendix A2. In all comparisons the statistical significance is estimated using a randomised resampling

140 ("bootstrapping with replacement") method. Correlations are calculated on random samples drawn from the entire simulation and the process is repeated 10,000 times to evaluate the likelihood of obtaining a significant relationship by chance.

3 Results

The tropical precipitation response to the QBO phase is analysed in both observations and model simulations, first in the annual-mean and then by season (section 3.1). The potential for aliasing with the ENSO signal is investigated (section 3.2) and

145 QBO-ENSO interactions are further explored (section 3.3), as well as QBO interactions with the Indian Ocean dipole (IOD). Finally, interactions between the QBO and the ITCZ, monsoons and the Walker circulation are identified and discussed in section 3.4.

3.1 Precipitation

QBO composite differences in annual mean precipitation (QBO-W minus QBO-E) are shown in Figure 1 from the gridded

150 GPCP observational dataset and from all three model simulations. In the observations the QBO signals are largest and statistically significant in the tropical Pacific, equatorial Atlantic and Indian Oceans, in good agreement with previous analyses (Liess and Geller, 2012; Gray et al., 2018). The three simulations agree reasonably well with the GPCP distributions and amplitudes, particularly in the Pacific and Indian Oceans. Positive differences of up to 1.2 mm day^{-1} are found in the equatorial Central
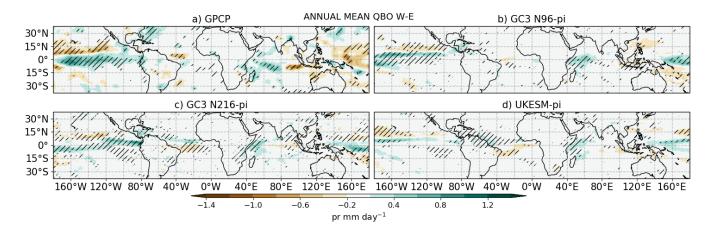
Figure 1. QBO-W minus QBO-E composite differences in annual-mean precipitation from (a) GPCP, (b) GC3 N96-pi, (c) GC3 N216-pi and (d) UKESM-pi. Hatching denotes statistically significant differences at the 95% confidence level using a bootstrapping with replacement test.

Pacific and the Indian Ocean and negative differences of up to 0.6 mm day^{-1} in the off-equatorial North Pacific, although the
differences are smaller in the simulations than observed.

In the tropical Atlantic, however, there is an indication of a weak but significant signal in the observations near the ITCZ but the models show a signal of the opposite sign in this region (or the absence of a signal in the case of GC3 N96-pi). This disagreement with observations may be due to the biased southward position of the Atlantic ITCZ in the model which is more pronounced in DJF (García-Franco et al., 2020).

The QBO signal in precipitation is found to be strongly dependent on the seasonal cycle in both models and observations. Figure 2 shows a comparison of the GPCP dataset and GC3 N216-pi for individual seasons (see Figure S1 for corresponding fields from the other models). The positive equatorial Pacific signal in the GPCP dataset, which resembles an El Niño anomaly, is particularly strong and statistically significant in December-January-February (DJF) (Fig. 2a). A similar pattern is present in both March-April-May (MAM) (Figure 2c) but with no statistical significance. In GC3 N216-pi the QBO signal in the Pacific is significant in all seasons, likely due to the greater number of years in the ensembles, although it is shifted slightly compared to GPCP and is strongest in MAM (Fig. 2c).

In the Atlantic, the QBO signal in the ITCZ region is more clearly evident in the individual seasons. In DJF there is reasonable similarity between the model and observations but by MAM the opposite sign of the model compared to GPCP becomes evident, even though the ITCZ bias in the model is stronger in DJF than in MAM (García-Franco et al., 2020). In addition, all models and GPCP indicate that the Caribbean Sea is wetter in JJA during QBO-W than in QBO-E (see Figs. 2 and S1). In the Indian Ocean, the observations and all models show relatively large and significant differences in SON, (Fig. 2e-f), characterized by a dipole of wet anomalies to the west and dry anomalies to the east. The dipole anomalies suggest a possible QBO influence on the IOD, which is characterized by a zonal gradient of SSTs and convective activity in the Indian Ocean that
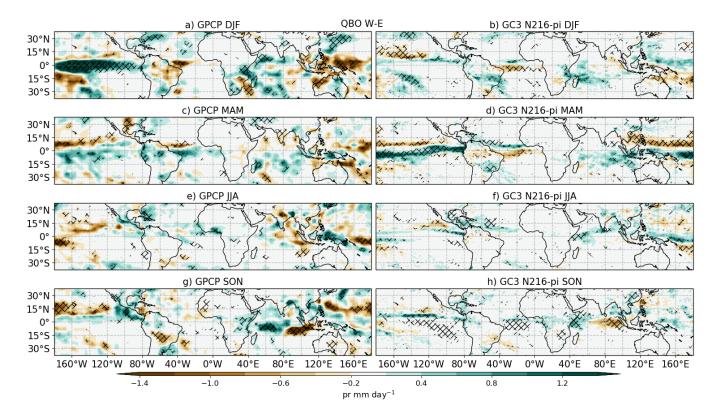
Figure 2. As in Figure 1, but showing seasonal-mean QBO composite from (left) GPCP and (right) GC3 N216-pi for DJF, MAM, JJA and SON from top to bottom.

is specially prominent in SON (Saji et al., 1999; Deser et al., 2010; McKenna et al., 2020). This possibility is explored further
175 in section 3.3 below.

In summary, the GPCP total precipitation composite analyses are consistent with previous analyses (Liess and Geller, 2012;
Gray et al., 2018). These composites show a zonally asymmetric QBO signal primarily in the ITCZ regions over the oceans.
The modelled QBO response patterns are in good agreement with the GPCP analysis albeit with small shifts in the timing of
the maximum response in the Pacific and in the latitude of the maximum Atlantic response. This good agreement, together with
180 the extended duration of the model simulations (500 years) compared with the available observations, suggests that analysis of
the modelled QBO signals may help to understand the mechanisms that give rise to the QBO signals at the surface. However,
the QBO signals from both model and observational analyses show strong similarities to well-known response patterns for
ENSO and the IOD. This highlights a possible interaction of the QBO with these phenomena. Previous observational studies
have also shown a higher frequency of El Niño events during QBOW and of La Niña during QBOE in observations since 1979
185 (Taguchi, 2010; Liess and Geller, 2012), although the observational record is short so there is much statistical uncertainty.
There is therefore potential for aliasing of the signals, which needs further investigation.
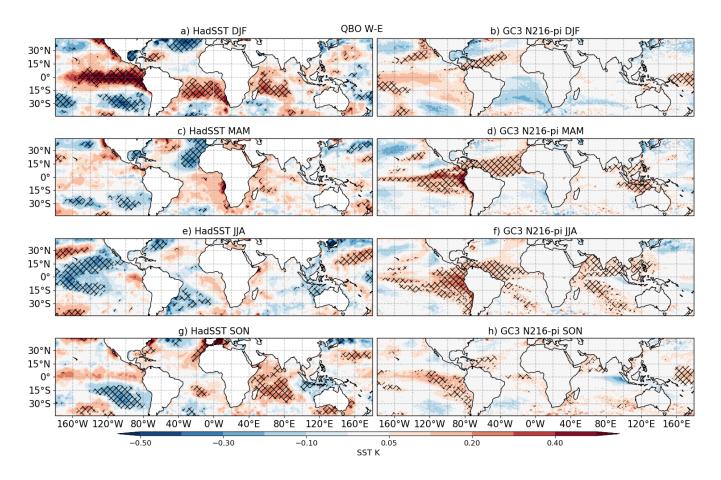
Figure 3. As in Figure 2 but for seasonal-mean sea surface temperatures from (left) the HadSST dataset and (right) GC3 N216-pi simulation.

3.2 Potential aliasing of QBO and ENSO signals

To further explore the QBO signal and its interaction with ENSO, Figure 3 shows the QBO signal in SSTs. The QBOW minus QBOE composite differences are shown for individual seasons from the HadSST dataset and the GC3 N216-pi model simu-

190   lation. The SST signals are consistent with the precipitation signals. Both model and observational datasets show significant positive SST responses in the equatorial Pacific that are similar to El Niño patterns. In the HadSST dataset the Pacific response is strongest in DJF and resembles an East Pacific (or 'standard') El Niño, whereas the simulated anomalies in DJF (for all models, see Fig. S2) are weaker and look more like a central Pacific El Niño (Capotondi et al., 2015).

     In GC3 N216-pi, the largest differences are observed in MAM in the easternmost Pacific Ocean and thus more closely

195   resembles the observed DJF response pattern. In the South Atlantic the model shows a region weak, insignificant cooling in DJF (Figure 3d), in contrast to the statistical significant warming signal in HadSST (Figures 3a,c). In the northern tropical Atlantic the model shows an year-long warming signal with stronger anomalies in MAM and JJA; this signal is present in
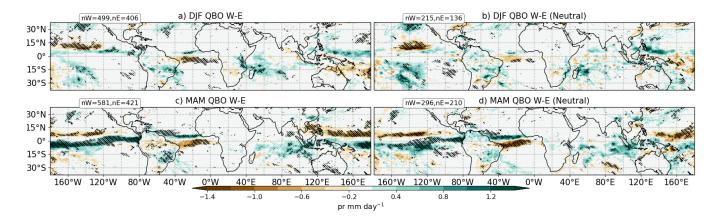
Figure 4. Composite QBO W-E differences of total precipitation in GC3 N216-pi in (a, b) DJF and (c, d) MAM for (a, c) all the events and (b, d) Neutral ENSO conditions only. The sample size of each composite is noted in the top left corner of each panel. Statistically significant differences to the 99% confidence level are shown through the hatching.

HadSST but only found in JJA and SON and it is not significant (Fig. 3e, g). The simulated northern tropical Atlantic warm anomalies in DJF (Figure 3b) are accompanied by a warmer Caribbean Sea and a cooling of the Gulf of Mexico, warmer SSTs

200 along the coast of California and a cooling of the central North Pacific, all of which resemble the impact of El Niño events and the positive phase of the Pacific North American (PNA) pattern (Deser et al., 2010; Guo et al., 2017; Jiménez-Esteve and Domeisen, 2020).

As an initial investigation of the possibility of aliasing between the QBO and ENSO signals, Figures 4a,b shows the DJF QBOW minus QBOE composite differences of total precipitation from the GC3 N216-pi simulation using all years (as in figure

205 2) compared with using only those years identified as 'ENSO-neutral'. Although the sample size is substantially reduced in the latter (see figure for the number of months in each QBO composite) the sample size is nevertheless still large (>120 data points in each composite). The response patterns are similar in each plot, which suggests that the QBO signal is unlikely to be the result of a sampling bias that favours one particular phase of ENSO.

An alternative approach to investigate the possibility of aliasing of the QBO/ENSO signals is to use a multi-linear regression

210 technique (see section 2) in which the signal is analysed for both QBO and ENSO simultaneously. Here, we switch to analysing convective precipitation to better investigate the possible influence of the QBO on deep tropical convection.

Figures 5a,b show results from a simple linear regression analysis of the monthly-averaged time-series of GC3 N216-pi total precipitation in which a single QBO index is employed. Figure 5a includes all available years while Figure 5b includes only neutral ENSO years. The results are very similar to the annual-mean composite differences in total precipitation (1), with

215 increased convective precipitation over the equatorial Pacific when the zonal winds at 70 hPa are positive.

Figures 5c,d show the ENSO and QBO signals when the Nino3.4 index is included as well as the QBO index. The ENSO response is clearly evident, highly statistically significant and compares well with the well-known patterns obtained from observations. The amplitude of the ENSO signal is also much larger than the QBO signal. Nevertheless, the QBO signal
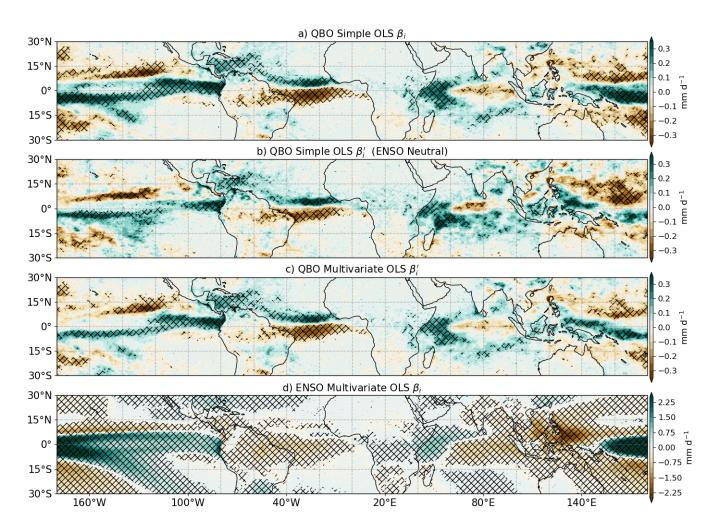
Figure 5. Annual-mean regression model results in GC3 N216-pi for convective precipitation. (a, b) Regression coefficients (β_i) from a simple ordinary least-squares (OLS) regression model with the QBO index for (a) all months and (b) ENSO-Neutral months only. (c, d) show the regression coefficients resulting from a multivariate regression model using the ENSO and QBO indices for the (c) QBO and (d) predictors. In all cases, the regression coefficients are rescaled by multiplying the regression coefficients with the ratio of maximum amplitude and standard deviation of the QBO or ENSO indices.

remains intact and all of the main features are still significant (Fig. 5c). For example, the positive regression coefficients that
220 suggest a northward shift of the Atlantic ITCZ and the wetter Caribbean Sea and western Indian Ocean in the simple regression
model are still found in the multivariate regression analysis. A similar analysis of tropical SSTs (Fig. S3) shows a QBO signal
in SSTs that is separate from the effect of ENSO and agrees with the results of the composite analysis (Fig. 3).

These results suggest that the modelled QBO signal in total precipitation does not arise due to a simple aliasing of the signal
with ENSO. However, the multi-linear regression technique assumes that the QBO and ENSO indices are orthogonal and that
225 their responses add together linearly. The similarity of the two responses indicate that this is clearly not the case and there
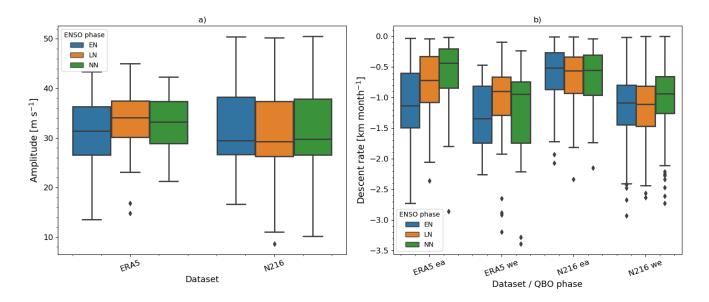
Figure 6. Box plots of QBO (a) amplitude [m s^{-1}] and (b) descent rate [km month^{-1}] separated by dataset (ERA5 and GC3 N216-pi) and ENSO phase. NN stands for Neutral ENSO. In (b) descent rates are shown for both descending easterly (ea) and westerly (we) phases following Schenzinger et al. (2017).

is substantial interaction between the two phenomena. Nevertheless, the QBO signal remains even when only neutral-ENSO years are included in the analysis, suggesting that the QBO has a real influence on the surface precipitation.

3.3 Interaction of the QBO with ENSO and IOD

To further explore the interaction of the QBO and ENSO, we first investigate whether aspects of the QBO are influenced by
230   ENSO events. This relationship could be a real possibility since the intrinsic mechanism of the QBO involves tropical waves that are generated within the troposphere. Schirber (2015) found in a GCM that under El Niño conditions tropospheric wave activity increases and accelerates the downward propagation speed of the QBO westerly phase. However, the analysis by Serva et al. (2020) shows that only models with high resolution can reproduce the observed ENSO effects on the QBO amplitude while several models show no impact of ENSO on the QBO.

235   For that reason, we analyse several characteristics of the QBO and their dependence on ENSO phase, namely the descent rate and the amplitude of the QBO (see the 'Methods and Data' section for details of how the QBO amplitude is defined). The results are summarised in Figure 6 for the ERA5 reanalysis dataset (35 years; 1979 – 2014) and for the GC3 N216-pi simulation (500 years). In ERA5, the well-known faster descent rates during the westerly phase than in the easterly phase is clearly evident and agrees well with studies of longer datasets such as the Berlin radiosonde data (Schenzinger et al., 2017).
240   Also, the ERA5 QBO descent rates and the amplitude both depend on the phase of ENSO. A higher amplitude and slower descent rates are observed during La Niña phases and weaker amplitudes and faster descent rates during El Niño.

Table 1. ENSO and IOD events frequency (month month^{-1}). For positive and negative events, for each mean value the error shown is the standard deviation of the probability density distribution (PDF) found by boostrapping with replacement. Results in **bold** indicate that the event frequency PDF for QBOW is significantly different to QBOE to the 95% confidence level according to the KS test.

Dataset	QBO phase	El Niño	La Niña	IOD+	IOD-
GC3 N216-pi	W	**0.24±0.09**	**0.19±0.05**	**0.17±0.03**	**0.11±0.02**
GC3 N216-pi	E	**0.21±0.07**	**0.26±0.07**	**0.12±0.03**	**0.15±0.03**
ERA5/HadSST	W	0.28±0.01	0.27±0.02	0.17±0.01	0.13±0.01
ERA5/HadSST	E	0.17±0.02	0.27±0.03	0.12±0.01	0.19±0.03

In the model, the descent rates are also faster for the westerly than the easterly QBO phase, as observed, but the relationship between the QBO characteristics and ENSO is less clear. Neither the amplitudes nor descent rates of the QBO are significantly different between El Niño (EN) and La Niña (LN) phases. Interestingly, the only significant difference in the model is that
245 descending westerlies are slower in Neutral ENSO months compared to EN or LN conditions, perhaps suggesting that tropical wave activity is increased in both ENSO phases compared with neutral years. The model results therefore suggest that there is little influence of ENSO on the descent rate and amplitude of the QBO in the GC3 N216-pi simulation. This finding of a null influence of ENSO on the QBO agrees well with the results of Serva et al. (2020) that examined these relationships in an older version of the HadGEM model. In summary, there is no evidence to suggest an influence of ENSO on the QBO in the model.
250 The reversed possibility, that the QBO may somehow influence ENSO events is now examined. A higher frequency of EN events during QBOW and of LN during QBOE has previously been noted (Taguchi, 2010; Liess and Geller, 2012) although the short observational record means that there is statistical uncertainty. In Table 1 we document the frequency of ENSO events in each QBO phase from the ERA5 reanalysis dataset and from the GC3 N216-pi simulation. Probability density functions (PDFs) were constructed for the model data using 36-yr samples with replacement and a Kolmogorov–Smirnov (KS) test was
255 used to evaluate if the PDFs of an event frequency (e.g. El Niño) were distinguishable for each phase of the QBO.

The results show significant differences for each ENSO phase in GC3 N216-pi (and this is also the case for the GC3 N96-pi and UKESM-pi simulations, not shown). El Niño events are more frequent under QBOW conditions than under QBOE in both observations and model datasets. La Niña events are equally frequent in both QBO phases in the HadSST dataset but in GC3 N216-pi they are more frequent under QBOE than under QBOW.
260 Figure 7a,b shows the ENSO3.4 index amplitude and interannual standard deviation as a function of each month from the HadSST dataset and the GC3 N216-pi simulation, separated for each phase of the QBO. From this we can examine, for example, whether any QBOW minus QBOE differences in ENSO characteristics arise primarily from one QBO phase or the other (i.e. a non-linear response) or whether both phases contribute equally to the response difference. There are significant QBO differences in EN3.4 SST in both the HadSST and GC3 N216-pi datasets. In particular, the mean ENSO indices are very
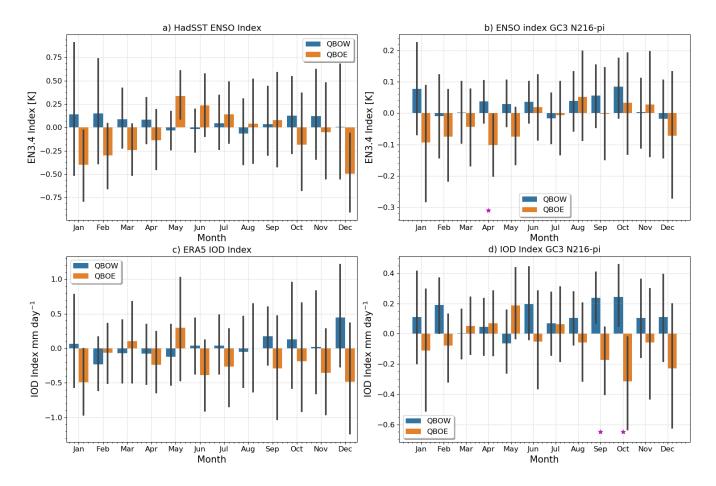
Figure 7. Monthly-mean (a-b) ENSO and (c-d) IOD-prc indices separated per QBO phase in (a, c) observations/reanalysis and (b, d) GC3 N216-pi. The error bars show the standard deviation of each index for each month and significant differences between QBO W and E months are highlighted with a ∗ at the bottom of each panel.

frequently positive in QBOW and negative in QBOE months from September until January. In the model, the differences are largest from Feb-to-May (in good agreement with the results shown in Figure 2).

Figure 7 also suggests substantial non-linearities in the QBO-ENSO interactions, since the amplitude of the EN3.4 anomaly in each month under QBO E/W conditions is seldom equal and opposite. This non-linearity is also evident in Figure 8 where the QBO composite differences in convective precipitation during the peak ENSO season (November through to March) are shown using all years, Neutral ENSO years and EN or LN years. While the broad nature of the QBO signal remains similar, the details differ depending on the phase of ENSO (8c,d). For example, the Atlantic ITCZ response is most prominent in Neutral and LN phases (Figure 8c) whereas the eastern off-equatorial Pacific drier response is only found under Neutral ENSO years.

Positive differences in the western Indian Ocean and in the northern tropical Pacific are much stronger during LN (Fig. 8d) than in other ENSO phases. These results can be interpreted as EN and LN teleconnections being slightly different for
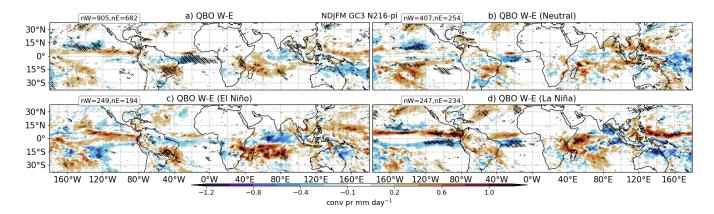
13

Figure 8. Composite QBO W-E convective precipitation differences of total precipitation in GC3 N216-pi in the season (NDJFM) for (a) all the events and (b) Neutral ENSO conditions only, (c) El Niño and (d) La Niña. The sample size of each composite is noted in the top left corner of each panel. Statistically significant differences to the 99% confidence level are shown through the hatching.

275 each QBO phase. For example, in South America, more specifically in the South Atlantic Convergence Zone region (Carvalho et al., 2004; Jorgetti et al., 2014), wetter conditions during QBOW compared to QBOE are found in all years but this difference appears stronger during EN events. Similarly, the western Indian Ocean and eastern Africa show positive significant differences (W-E) during LN. These results suggest that in this model simulation, ENSO impacts to South America, Eastern Africa and the Indian Ocean are also dependent on the QBO phase.

280 Returning to Figure 7, during Dec-March in HadSST and Jan-May in GC3 N216-pi the QBO signal comes primarily from the QBOE phase, since the EN3.4 amplitudes are near zero under QBOW in these months. These results are consistent with the analysis of ENSO frequency in Table 1, which shows more frequent La Niña events under QBOE and El Niño events under QBOW. These results also suggest, therefore, that a stronger amplitude La Niña event in DJF may develop if there is a QBOE phase present in the lower stratosphere.

285 In the previous sections the precipitation and SST analyses also showed suggestive evidence of a relationship between the QBO and the IOD, in both the observations and the model. A link between the QBO and the IOD index and event frequency have been analysed in the same way as for the ENSO index and a significant relationship is confirmed (Table 1 and Figs. 7c-d). The model results indicate a more frequently positive IOD index under QBOW and a negative index for QBOE, and these differences are statistically significant in September and October. The GC3 N96-pi and UKESM-pi results are very similar (Fig.
290 S4) and the differences are also significant. The IOD event frequency is also markedly different depending on the QBO phase, with positive events more frequently observed in the westerly phase of the QBO and negative events found more frequently under QBOE, both for ERA5 and the model simulations (Table 1).

This section demonstrates statistically robust links between the IOD and ENSO, and the QBO. ENSO and the IOD are intertwined with pan-tropical teleconnections through zonal circulations (Cai et al., 2019), monsoons and the ITCZ. For that
295 reason, the following section explores more closely the links between the QBO and features of the tropical circulation.
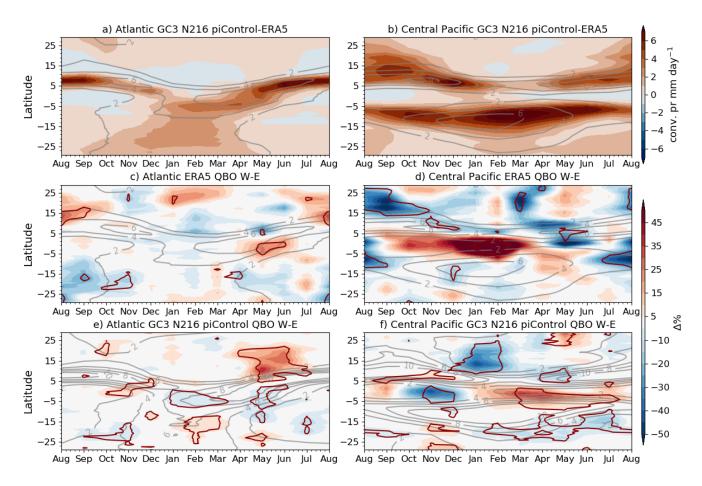
Figure 9. (a, b) Zonal mean biases in convective precipitation in GC3 N216-pi compared to ERA5 in the (a) Atlantic [60°W-20°W] and (b) Central Pacific [180°W-140°W] sectors. (c-f) Monthly and zonal mean QBO W-E percent (%) differences in convective precipitation where the absolute difference is weighted by the climatological value at each latitude and month. The line-contour (red) depict differences that are statistically significant to the 95% level according to a bootstrapping test and the grey lines show the climatological values.

3.4 ITCZ, monsoons and the tropical circulation

This section investigates how the ITCZ, monsoons and the Walker circulation are influenced by the QBO in the model compared to the observations. Climate model biases in the representation of the migration and dynamics of the ITCZ, or in the mean-state of the Walker circulation, may modify any physical effects of the QBO over convection. For example, ITCZ biases in position 300 or strength (Fig. 9a-b) are noteworthy in the model, and are mainly characterized by a southward shift of the simulated Atlantic ITCZ in DJF and MAM and a wider extent of the Central Pacific ITCZ compared to ERA5.

The monthly-mean QBO W-E zonal-mean convective precipitation differences in the Pacific and Atlantic ITCZ regions (Figure 9) show that the ITCZ impacts are seasonally dependent. While there are no clear differences in the Atlantic sector
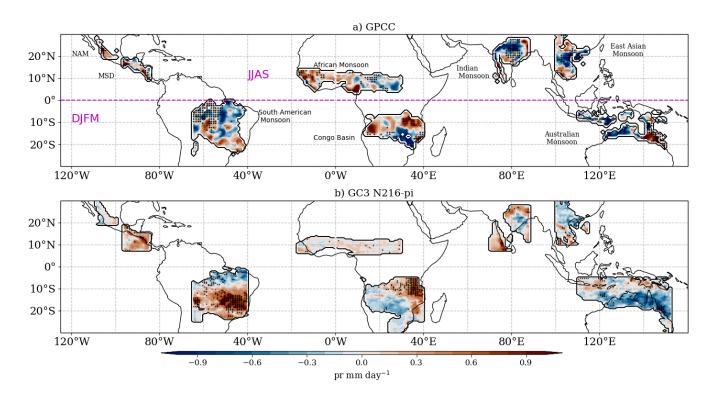
15

Figure 10. Convective precipitation differences in monsoon regions between QBO W-E phases for a) ERA5 and b) GC3 N216-pi. For monsoon regions in the Northern hemisphere, differences are shown for the JJAS period, whereas for Southern Hemisphere monsoons, results are shown for DJFM. Red dots indicate differences that are statistically significant to the 95% level according to the bootstrapping test.

for ERA5 in any month, in GC3 N216-pi there is a significant northward shift of the ITCZ from April to June, which is likely associated with the warm SST anomalies found in this season in the northern tropical Atlantic (Fig. 3).

The differences in the Pacific sector confirm previous model and observational results (Gray et al., 2018; Serva et al., submitted) that the Pacific ITCZ becomes stronger and shift southward during QBOW compared to QBOE (Fig. 9d, f). In observations, the strongest differences are found during DJF, characterized by increased precipitation over the core ITCZ regions. In GC3 N216-pi, a southward shift of the ITCZ is observed from February to July, maximized in the MAM season. Very similar results for the Atlantic and Pacific sectors were observed for the other two simulations (not shown). The result also holds for ENSO Neutral periods (Fig. S5) which rules out the possibility that the Atlantic ITCZ results are due to ENSO teleconnections to the tropical north Atlantic.

In spite of existing observational evidence (Collimore et al., 2003; Liess and Geller, 2012; Gray et al., 2018) that suggests a link between the QBO and monsoon regions, the results in the previous sections (Fig. 1) show little-to-no effect of the QBO on precipitation over land in the simulations. The precipitation response over land is examined more closely by analysing regions that fit the concept of the global monsoon. For this purpose, a monsoon region is defined as a region in which over 55% of the

total annual rainfall is observed or simulated in the respective summer season and the summer-winter rainfall rate difference is higher than 2 mm day^{-1} (Wang and Ding, 2008; Wang et al., 2017, 2021).

After defining these regions, the QBO W-E differences are computed for JJAS and DJFM for Northern and Southern Hemisphere monsoons, respectively. Figure 10 shows that there is no coherent response to the QBO phase in GPCC in any monsoon region. However, in GC3 N216-pi there are significant differences for Southern Hemisphere monsoons. In the South American monsoon region, the QBO W-E differences indicate a significantly wetter region in South America, where the South Atlantic Convergence Zone is located (Carvalho et al., 2004; Jorgetti et al., 2014). Similarly, a drier Australian monsoon and wetter conditions for East Africa are observed during QBOW compared to QBOE.

For Northern Hemisphere monsoons there are no robust or significant differences (Fig. 10b). However, when only Neutral ENSO months are considered, all three simulations suggest a wetter Central American monsoon (not shown) in QBOW compared to QBOE. The different responses observed for the three simulations suggest that the representation of the dynamical features of each monsoon by each model configuration is important for any response to the QBO. Furthermore, the relatively
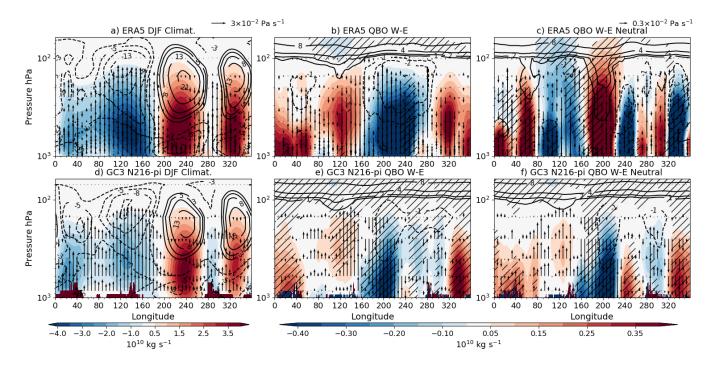

Figure 11. (a, d) Climatological mean-state of the Walker circulation, depicted through the zonal streamfunction (ψ) in shading, the zonal wind (contours), and vertical velocity (ω [Pa s^{-1}], vectors) during the DJF season in a) ERA5 and (b) N216-pi. (b, c, e, f) show W-E composite differences, during DJF, for the same variables only that hatching represents statistical significance to the 95% confidence level for differences in the streamfunction, and only statistically significant differences in the zonal wind and ω are shown. (g-h) are as in (d-f) but considering Neutral ENSO periods only. Example vector sizes for ω are given in the top right corners of a and c.

17

smaller signals seen over land compared to over the oceans suggests that SST feedbacks are important for the QBO response
330   in the model, so that reduced impacts are seen in regions of land convection.

A number of studies have suggested a link between the QBO and the Walker circulation to explain the zonally asymmetric
nature of the QBO anomalies in convective precipitation (e.g. Collimore et al., 2003; Liess and Geller, 2012). To evaluate this
hypothesis, the zonal streamfunction is used to measure the Walker circulation (Yu and Zwiers, 2010; Bayr et al., 2014) and is
defined as:

$$\psi = 2\pi \frac{a}{g} \int_0^p u_D dp, \tag{1}$$

335

where ψ is the zonal streamfunction, u_D is the divergence part of the zonal wind, a is the Earth's radius, p is the pressure
coordinate and g the gravitational constant. The streamfunction is calculated by first averaging over the equatorial band of
10°S-10°N and integrating to the top level of each dataset.

QBOW minus QBOE composite differences in DJF show that the streamfunction in the eastern Pacific [220-260°E] is
340   significantly weaker during QBOE than during QBOW in ERA5 and GC3 N216-pi (Fig. 11). These streamfunction differences
are significant even low in the troposphere in the model. The zonal wind at upper-levels (300-100 hPa) is also weaker in
QBOW compared to QBOE at 200°E in both model and reanalysis. In GC3 N216-pi, the negative ψ difference is accompanied
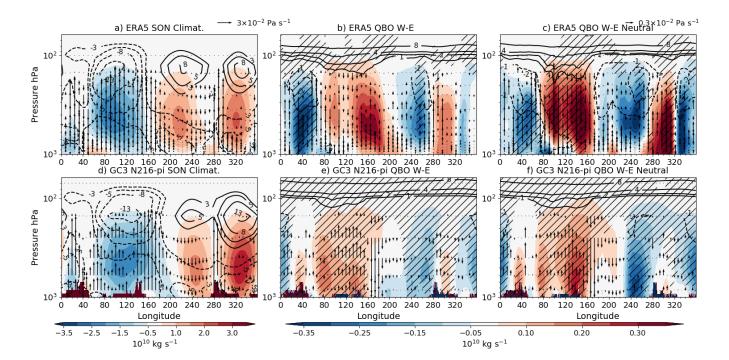

Figure 12. As in Figure 11 but for the SON season.

by descending motion anomalies in the 170-220°E region, whereas anomalous ascent is observed in the Maritime continent and Indian Ocean. The differences in the other simulations agree with the results of GC3 N216-pi (not shown).

345   In boreal fall (Fig. 12), the differences are also significant and are linked to the relationships found between the IOD and the QBO. Specifically, significant positive differences in the streamfunction are found in the eastern Indian Ocean and maritime continent and negative differences in the eastern Pacific. In GC3 N216-pi, vertical velocity anomalies indicate stronger ascent in the western Indian Ocean and in the Maritime continent whereas descending anomalies are found in the eastern Indian Ocean. These results agree with positive IOD indices found in QBOW and a mean negative index during QBOE.

350   The rightmost panels in Figures 11 and 12, in which only Neutral ENSO months are considered, suggest that this relationship between the QBO and the Walker circulation occurs regardless of ENSO events for GC3 N216-pi. However in ERA5, removing ENSO events changes the sign of the response, likely due to the small sample size in the observational record when only neutral months are considered. These results highlight links between the large-scale overturning circulation and local responses which may explain the zonally asymmetric results found in previous studies and in early sections of this paper.

355 **4   Summary and discussion**

Analyses of observational records of precipitation suggest links between the stratospheric QBO and the surface tropical climate (Collimore et al., 2003; Liess and Geller, 2012; Gray et al., 2018). However, the short available observational record (<40 years) and the confounding influence of ENSO and its teleconnections limits the robustness of any analysis seeking to explore these links and possible mechanisms of interaction between the QBO and tropical surface climate. This study investigates the tropical

360 signature of the QBO in the 500-year-long pre-industrial control CMIP6 experiments of the Met Office Hadley Centre Unified Model, with a focus on the HadGEM3 GC3.1 N216 simulation.

     Composite and regression analyses were used to demonstrate the presence of a statistically significant link between the QBO and the position and strength of the Pacific ITCZ, the Atlantic ITCZ, precipitation variability in the Caribbean Sea and the Indian Ocean, as well as Southern Hemisphere monsoon regions. The QBO signal was found to be zonally asymmetric, with the

365 more robust and largest differences over the oceans, suggesting the possibility of SST feedback processes. The modelled QBO signals agree well with observational analyses and the length of the simulation allows for improved estimation of statistical significance and further exploration of the possible source of these signals.

     The possibility of aliasing of the QBO and ENSO signals and their interaction was extensively explored, using the model simulations. When only ENSO-neutral years are analysed the QBO signal remains essentially unchanged, ruling out the pos-

370 sibility of a straightforward aliasing of ENSO events with the QBO phase selection. The possibility that the apparent QBO signature at the surface is due to an ENSO bias in selection of the QBO phase was also considered. An influence of ENSO on the descent rate and amplitude of the QBO, via modulation of tropical wave generation, has been proposed (Schirber, 2015). However, while the model was found to successfully simulate the well-known difference in QBO descent rates in which the QBOW phase descends more rapidly than the QBOE phase, there was no evidence for an ENSO influence on the rate of descent

375 or amplitude of either QBO phase.

This analysis therefore provides evidence for a QBO influence on tropical surface climate that is not simply due to aliasing or a bias in how the QBO index is determined. However, the QBO response patterns strongly suggest that any QBO influence is likely to involve processes such as deep convection and tropical circulation patterns that are also influenced by ENSO. Potential pathways of interaction between the QBO and ENSO signals were therefore explored. While recognising that linear diagnostics are unable to provide specific evidence of cause and effects, they may nevertheless identify candidate mechanisms that are worth exploring more fully.

The frequency of ENSO events in each phase of the QBO was first explored. In observations, El Niño events have been found to occur more frequently in QBOW years and La Niña events are more frequently found in QBOE years (Taguchi, 2010), suggesting a non-linear interaction of ENSO with the QBO. This dependence was successfully reproduced in the model, providing supporting evidence that the observed QBO-ENSO relationship is not due to observational uncertainty. Similarly, examination of month-by-month ENSO amplitude and interannual variability in the model showed that the interaction between QBO and ENSO is far from linear, since the amplitude dependence on QBO phase was asymmetric. The non-linearity of the QBO-ENSO interaction was confirmed using composite analyses that showed different QBO signal patterns during El Niño years as compared with La Niña years.

In addition to the QBO-ENSO link, the model analysis of total precipitation also highlighted a statistically significant QBO signal in the Indian Ocean, raising the possibility of an interaction with the Indian Ocean Dipole (IOD). In boreal fall the IOD index, which measures the zonal gradient of precipitation in the Indian Ocean, was found to be anomalously positive in QBOW years and anomalously negative in QBOE years.

Finally, the QBO signal in the Walker circulation, the ITCZ and monsoon circulations were investigated in the model. Previous studies have proposed that the QBO may influence the mean-state of the Walker circulation, which could explain the zonally asymmetric nature of the QBO signal in precipitation in the tropics (Collimore et al., 2003; Liess and Geller, 2012; Hitchman et al., 2021). The modelled Walker circulation was found to vary by up to 10% between QBO phases, even when the effect of ENSO events was taken into account. Specifically, the Walker circulation was found to be weaker during QBOW than during QBOE. In DJF, this anomaly of the overturning circulation in the Pacific is likely linked to the stronger East Pacific ITCZ, and in SON, the changes to the overturning are likely linked to the ascending and descending motions in the Indian Ocean that generate the IOD response.

The East Pacific and Atlantic ITCZ, as well as monsoons, show a sensitivity to the QBO phase in observations (Gray et al., 2018; Hitchman et al., 2021) and some of these connections are also found in this model study. Most Southern Hemisphere monsoons show a robust and significant response to the QBO but in the Northern Hemisphere only the Central American rainfall was robustly linked to the QBO. The weaker response over land monsoon regions than over oceanic features such as the ITCZ further underscores the possible relevance of SST feedbacks.

The robust connections diagnosed in this study warrant further analysis as multiple questions remain open regarding the mechanisms that disentangle the cause and effect of these relationships. Targeted model experiments are needed to investigate hypotheses, such as the static stability mechanism (Hitchman et al., 2021), and disentangle the direction of causality between the tropical stratosphere and troposphere. Additionally, further model experiments may also help to understand why the MJO-

QBO connections are not found within the MOHC model whereas other observed responses are reasonably well reproduced by the model.

Appendix A: Methods

A1 Weighted average for composites

The seasonal and annual-mean composites were derived by weighting each observations by the relative size of each month to the total composite size and by the number of days in the month of each observation relative to the total number of days in the composite period. This procedures ensures that all observations that all months contribute equally regardless of whether one month has more days or whether more observations are found in a month within a composite. An equation for this procedure can be written as:

$$\bar{X} = \sum_{i}^{N} x_i \cdot w_i(m) \tag{A1}$$

where $\bar{X}$ is the target composite mean of a quantity, N is the total observations that qualify for the composite, i indexes all the observations, $w_i(m)$ is the corresponding weight for each observation which is a function of the month (m). The weighting function $w_i(m)$ is then given by:

$$w_i(m) = \frac{d_m}{d_t} \frac{1}{s_m} \tag{A2}$$

where s_m is the sample size of observations for month m, d_t is the total number of days possible for the composite, e.g., $d_t = 365$ for annual means and d_m is the number of days in the month m, e.g., for January $d_m = 30$ days and for February $d_m = 28$ days.

A2 Regression analysis

The simple linear regression model can be written as:

$$Y(t) = X_0 + X_i(t)\beta_i + \epsilon, \tag{A3}$$

where Y is the measured or dependent variable, X_0 is a constant coefficient, β_i is the regression coefficient between X_i and Y and ϵ represents random error or a residual. In all cases, the models were solved using an ordinary least-squares (OLS) method. A multivariate regression model was used to study the joint effect of two or more predictors, in this case ENSO and QBO indices, over a variable (Y), in this case precipitation, such that the model can be written as:

$$Y(t) = X_0 + \sum_{j}^{N} X_j(t)\beta_j + \epsilon \tag{A4}$$

where $X_j(t)$ is any predictor with an associated regression coefficient β_j.

As in previous studies (Gray et al., 2018; Misios et al., 2019), the regression coefficient can be rescaled to evaluate the total effect that a predictor (X_j) can have on the variance of the measured variable (Y) using the standard deviation (σ_j) and the maximum ($X_{j,max}$) and minimum ($X_{j,min}$) values of X_j so that the rescaled coefficient β'_j can be written as:

$$\beta'_j = \beta_j \frac{X_{j,max} - X_{j,min}}{\sigma_j}. \tag{A5}$$

A3

References

455 Abdelmoaty, H. M., Papalexiou, S. M., Rajulapati, C. R., and AghaKouchak, A.: Biases beyond the mean in CMIP6 extreme precipitation: A global investigation, Earth's Future, 9, e2021EF002 196, 2021.

Adler, R. F., Huffman, G. J., Chang, A., Ferraro, R., Xie, P.-P., Janowiak, J., Rudolf, B., Schneider, U., Curtis, S., Bolvin, D., Gruber, A., Susskind, J., Arkin, P., and Nelkin, E.: The version-2 global precipitation climatology project (GPCP) monthly precipitation analysis (1979–present), Journal of hydrometeorology, 4, 1147–1167, 2003.

460 Adler, R. F., Sapiano, M. R., Huffman, G. J., Wang, J.-J., Gu, G., Bolvin, D., Chiu, L., Schneider, U., Becker, A., Nelkin, E., et al.: The Global Precipitation Climatology Project (GPCP) monthly analysis (new version 2.3) and a review of 2017 global precipitation, Atmosphere, 9, 138, 2018.

Andrews, M. B., Knight, J. R., Scaife, A. A., Lu, Y., Wu, T., Gray, L. J., and Schenzinger, V.: Observed and simulated teleconnections between the stratospheric quasi-biennial oscillation and Northern Hemisphere winter atmospheric circulation, Journal of Geophysical
465 Research: Atmospheres, 124, 1219–1232, 2019b.

Anstey, J. A. and Shepherd, T. G.: High-latitude influence of the quasi-biennial oscillation, Quarterly Journal of the Royal Meteorological Society, 140, 1–21, 2014.

Anstey, J. A., Simpson, I. R., Richter, J. H., Naoe, H., Taguchi, M., Serva, F., Gray, L. J., Butchart, N., Hamilton, K., Osprey, S., et al.: Teleconnections of the Quasi-Biennial Oscillation in a multi-model ensemble of QBO-resolving models, Quarterly Journal of the Royal
470 Meteorological Society, 2021.

Bayr, T., Dommenget, D., Martin, T., and Power, S. B.: The eastward shift of the Walker Circulation in response to global warming and its relationship to ENSO variability, Climate dynamics, 43, 2747–2763, 2014.

Becker, A., Finger, P., Meyer-Christoffer, A., Rudolf, B., and Ziese, M.: GPCC full data reanalysis version 6.0 at 1.0: monthly land-surface precipitation from rain-gauges built on GTS-based and historic data, Global Precipitation Climatology Centre (GPCC): Berlin, Germany,
475 2011.

Becker, A., Finger, P., Meyer-Christoffer, A., Rudolf, B., Schamm, K., Schneider, U., and Ziese, M.: A description of the global land-surface precipitation data products of the Global Precipitation Climatology Centre with sample applications including centennial (trend) analysis from 1901–present, Earth System Science Data, 5, 71–99, 2013.

Cai, W., Wu, L., Lengaigne, M., Li, T., McGregor, S., Kug, J.-S., Yu, J.-Y., Stuecker, M. F., Santoso, A., Li, X., Ham, Y.-G., Chikamoto,
480 Y., Ng, B., McPhaden, M. J., Du, Y., Dommenget, D., Jia, F., Kajtar, J. B., Keenlyside, N., Lin, X., Luo, J.-J., Martín-Rey, M., Ruprich-Robert, Y., Wang, G., Xie, S.-P., Yang, Y., Kang, S. M., Choi, J.-Y., Gan, B., Kim, G.-I., Kim, C.-E., Kim, S., Kim, J.-H., and Chang, P.: Pantropical climate interactions, Science, 363, eaav4236, 2019.

Capotondi, A., Wittenberg, A. T., Newman, M., Di Lorenzo, E., Yu, J.-Y., Braconnot, P., Cole, J., Dewitte, B., Giese, B., Guilyardi, E., et al.: Understanding ENSO diversity, Bulletin of the American Meteorological Society, 96, 921–938, 2015.

485 Carvalho, L. M., Jones, C., and Liebmann, B.: The South Atlantic convergence zone: Intensity, form, persistence, and relationships with intraseasonal to interannual activity and extreme rainfall, Journal of Climate, 17, 88–108, 2004.

Christiansen, B., Yang, S., and Madsen, M. S.: Do strong warm ENSO events control the phase of the stratospheric QBO?, Geophysical Research Letters, 43, 10–489, 2016.

Claud, C. and Terray, P.: Revisiting the possible links between the quasi-biennial oscillation and the Indian summer monsoon using NCEP
490 R-2 and CMAP fields, Journal of Climate, 20, 773–787, 2007.

Collimore, C. C., Martin, D. W., Hitchman, M. H., Huesmann, A., and Waliser, D. E.: On the relationship between the QBO and tropical deep convection, Journal of climate, 16, 2552–2568, 2003.

Deser, C., Alexander, M. A., Xie, S.-P., and Phillips, A. S.: Sea surface temperature variability: Patterns and mechanisms, Annual review of marine science, 2, 115–143, 2010.

495 García-Franco, J. L., Gray, L. J., and Osprey, S.: The American monsoon system in HadGEM3 and UKESM1, Weather and Climate Dynamics, 1, 349–371, https://doi.org/10.5194/wcd-1-349-2020, 2020.

Garfinkel, C. I. and Hartmann, D.: Influence of the quasi-biennial oscillation on the North Pacific and El Niño teleconnections, Journal of Geophysical Research: Atmospheres, 115, 2010.

Garfinkel, C. I. and Hartmann, D. L.: The influence of the quasi-biennial oscillation on the troposphere in winter in a hierarchy of models.
500 Part II: Perpetual winter WACCM runs, Journal of the Atmospheric Sciences, 68, 2026–2041, 2011a.

Garfinkel, C. I. and Hartmann, D. L.: The influence of the quasi-biennial oscillation on the troposphere in winter in a hierarchy of models. Part I: Simplified dry GCMs, Journal of the Atmospheric Sciences, 68, 1273–1289, 2011b.

Giorgetta, M. A., Bengtsson, L., and Arpe, K.: An investigation of QBO signals in the east Asian and Indian monsoon in GCM experiments, Climate dynamics, 15, 435–450, 1999.

505 Gray, L. J., Anstey, J. A., Kawatani, Y., Lu, H., Osprey, S., and Schenzinger, V.: Surface impacts of the Quasi Biennial Oscillation, Atmospheric Chemistry and Physics, 18, 8227–8247, https://doi.org/10.5194/acp-18-8227-2018, 2018.

Gray, W. M.: Atlantic seasonal hurricane frequency. Part I: El Niño and 30 mb quasi-biennial oscillation influences, Monthly Weather Review, 112, 1649–1668, 1984.

Guo, Y., Ting, M., Wen, Z., and Lee, D. E.: Distinct patterns of tropical Pacific SST anomaly and their impacts on North American climate,
510 Journal of Climate, 30, 5221–5241, 2017.

Hansen, F., Matthes, K., and Wahl, S.: Tropospheric QBO–ENSO interactions and differences between the Atlantic and Pacific, Journal of Climate, 29, 1353–1368, 2016.

Haynes, P., HITCHCOCK, P., HITCHMAN, M., YODEN, S., HENDON, H., KILADIS, G., KODERA, K., and SIMPSON, I.: The influence of the stratosphere on the tropical troposphere, Journal of the Meteorological Society of Japan. Ser. II, 2021.

515 Hersbach, H., Bell, B., Berrisford, P., Hirahara, S., Horányi, A., Muñoz-Sabater, J., Nicolas, J., Peubey, C., Radu, R., Schepers, D., Simmons, A., Soci, C., Abdalla, S., Abellan, X., Balsamo, G., Bechtold, P., Biavati, G., Bidlot, J., Bonavita, M., De Chiara, G., Dahlgren, P., Dee, D., Diamantakis, M., Dragani, R., Flemming, J., Forbes, R., Fuentes, M., Geer, A., Haimberger, L., Healy, S., Hogan, R. J., Hólm, E., Janisková, M., Keeley, S., Laloyaux, P., Lopez, P., Lupu, C., Radnoti, G., de Rosnay, P., Rozum, I., Vamborg, F., Villaume, S., and Thépaut, J.-N.: The ERA5 global reanalysis, Quarterly Journal of the Royal Meteorological Society, 146, 1999–2049,
520 https://doi.org/10.1002/qj.3803, 2020.

Hitchman, M. H., Yoden, S., Haynes, P. H., Kumar, V., and Tegtmeier, S.: An observational history of the direct influence of the stratospheric quasi-biennial oscillation on the tropical and subtropical upper troposphere and lower stratosphere, Journal of the Meteorological Society of Japan. Ser. II, 2021.

Ho, C.-H., Kim, H.-S., Jeong, J.-H., and Son, S.-W.: Influence of stratospheric quasi-biennial oscillation on tropical cyclone tracks in the
525 western North Pacific, Geophysical Research Letters, 36, 2009.

Holton, J. R. and Tan, H.-C.: The influence of the equatorial quasi-biennial oscillation on the global circulation at 50 mb, Journal of the Atmospheric Sciences, 37, 2200–2208, 1980.

Huang, B., Hu, Z.-Z., Kinter, J. L., Wu, Z., and Kumar, A.: Connection of stratospheric QBO with global atmospheric general circulation and tropical SST. Part I: Methodology and composite life cycle, Climate dynamics, 38, 1–23, 2012.

530   Jaramillo, A., Dominguez, C., Raga, G., and Quintanar, A. I.: The Combined QBO and ENSO Influence on Tropical Cyclone Activity over the North Atlantic Ocean, Atmosphere, 12, 1588, 2021.

Jiménez-Esteve, B. and Domeisen, D. I. V.: Nonlinearity in the tropospheric pathway of ENSO to the North Atlantic, Weather and Climate Dynamics, 1, 225–245, https://doi.org/10.5194/wcd-1-225-2020, 2020.

Jorgetti, T., da Silva Dias, P. L., and de Freitas, E. D.: The relationship between South Atlantic SST and SACZ intensity and positioning,
535   Climate dynamics, 42, 3077–3086, 2014.

Kennedy, J., Rayner, N., Smith, R., Parker, D., and Saunby, M.: Reassessing biases and other uncertainties in sea surface temperature observations measured in situ since 1850: 2. Biases and homogenization, Journal of Geophysical Research: Atmospheres, 116, 2011.

Kim, H., Caron, J. M., Richter, J. H., and Simpson, I. R.: The Lack of QBO-MJO Connection in CMIP6 Models, Geophysical Research Letters, 47, e2020GL087 295, https://doi.org/10.1029/2020GL087295, e2020GL087295 2020GL087295, 2020.

540   Klotzbach, P., Abhik, S., Hendon, H., Bell, M., Lucas, C., Marshall, A., and Oliver, E.: On the emerging relationship between the stratospheric Quasi-Biennial oscillation and the Madden-Julian oscillation, Scientific reports, 9, 1–9, 2019.

Kuhlbrodt, T., Jones, C. G., Sellar, A., Storkey, D., Blockley, E., Stringer, M., Hill, R., Graham, T., Ridley, J., Blaker, A., Calvert, D., Copsey, D., Ellis, R., Hewitt, H., Hyder, P., Ineson, S., Mulcahy, J., Siahaan, A., and Walton, J.: The low-resolution version of HadGEM3 GC3. 1: Development and evaluation for global climate, Journal of advances in modeling earth systems, 10, 2865–2888, 2018.

545   Lee, J. C. K. and Klingaman, N. P.: The effect of the quasi-biennial oscillation on the Madden–Julian oscillation in the Met Office Unified Model Global Ocean Mixed Layer configuration, Atmospheric Science Letters, 19, e816, https://doi.org/10.1002/asl.816, 2018.

Liess, S. and Geller, M. A.: On the relationship between QBO and distribution of tropical deep convection, Journal of Geophysical Research: Atmospheres, 117, 2012.

Lim, Y., Son, S.-W., Marshall, A. G., Hendon, H. H., and Seo, K.-H.: Influence of the QBO on MJO prediction skill in the subseasonal-to-
550   seasonal prediction models, Climate Dynamics, 53, 1681–1695, 2019.

Liu, M., Ren, H.-L., Zhang, R., Ineson, S., and Wang, R.: ENSO phase-locking behavior in climate models: from CMIP5 to CMIP6, Environmental Research Communications, 3, 031 004, 2021.

Lu, H., Hitchman, M. H., Gray, L. J., Anstey, J. A., and Osprey, S. M.: On the role of Rossby wave breaking in the quasi-biennial modulation of the stratospheric polar vortex during boreal winter, Quarterly Journal of the Royal Meteorological Society, 146, 1939–1959, 2020.

555   Ma, T., Chen, W., Huangfu, J., Song, L., and Cai, Q.: The observed influence of the Quasi-Biennial Oscillation in the lower equatorial stratosphere on the East Asian winter monsoon during early boreal winter, International Journal of Climatology, 2021.

Martin, Z., Vitart, F., Wang, S., and Sobel, A.: The Impact of the Stratosphere on the MJO in a Forecast Model, Journal of Geophysical Research: Atmospheres, 125, e2019JD032 106, 2020.

Martin, Z., Son, S.-W., Butler, A., Hendon, H., Kim, H., Sobel, A., Yoden, S., and Zhang, C.: The influence of the quasi-biennial oscillation
560   on the Madden–Julian oscillation, Nature Reviews Earth & Environment, pp. 1–13, 2021b.

Martin, Z., Sobel, A., Butler, A., and Wang, S.: Variability in QBO temperature anomalies on annual and decadal time scales, Journal of Climate, 34, 589–605, 2021c.

McKenna, S., Santoso, A., Gupta, A. S., Taschetto, A. S., and Cai, W.: Indian Ocean Dipole in CMIP5 and CMIP6: characteristics, biases, and links to ENSO, Scientific reports, 10, 1–13, 2020.

565   Menary, M. B., Kuhlbrodt, T., Ridley, J., Andrews, M. B., Dimdore-Miles, O. B., Deshayes, J., Eade, R., Gray, L., Ineson, S., Mignot, J.,
       Roberts, C. D., Robson, J., Wood, R. A., and Xavier, P.: Preindustrial Control Simulations With HadGEM3-GC3. 1 for CMIP6, Journal of
       Advances in Modeling Earth Systems, 10, 3049–3075, 2018.

       Misios, S., Gray, L. J., Knudsen, M. F., Karoff, C., Schmidt, H., and Haigh, J. D.: Slowdown of the Walker circulation at solar cycle maximum,
       Proceedings of the National Academy of Sciences, 116, 7186–7191, 2019.

570   Nie, J. and Sobel, A. H.: Responses of tropical deep convection to the QBO: Cloud-resolving simulations, Journal of the Atmospheric
       Sciences, 72, 3625–3638, 2015.

       Peña-Ortiz, C., Manzini, E., and Giorgetta, M. A.: Tropical deep convection impact on southern winter stationary waves and its modulation
       by the quasi-biennial oscillation, Journal of Climate, 32, 7453–7467, 2019.

       Richter, I. and Tokinaga, H.: An overview of the performance of CMIP6 models in the tropical Atlantic: mean state, variability, and remote
575   impacts, Climate Dynamics, 55, 2579–2601, 2020.

       Richter, J. H., Anstey, J. A., Butchart, N., Kawatani, Y., Meehl, G. A., Osprey, S., and Simpson, I. R.: Progress in Simulating the
       Quasi-Biennial Oscillation in CMIP Models, Journal of Geophysical Research: Atmospheres, 125, e2019JD032 362, e2019JD032362
       10.1029/2019JD032362, 2020.

       Saji, N., Goswami, B. N., Vinayachandran, P., and Yamagata, T.: A dipole mode in the tropical Indian Ocean, Nature, 401, 360–363, 1999.

580   Schenzinger, V., Osprey, S., Gray, L., and Butchart, N.: Defining metrics of the Quasi-Biennial Oscillation in global climate models, Geosci-
       entific Model Development, 10, 2017.

       Schirber, S.: Influence of ENSO on the QBO: Results from an ensemble of idealized simulations, Journal of Geophysical Research: Atmo-
       spheres, 120, 1109–1122, 2015.

       Schneider, U., Becker, A., Finger, P., Meyer-Christoffer, A., Rudolf, B., and Ziese, M.: GPCC full data reanalysis version 6.0 at 0.5: Monthly
585   land-surface precipitation from rain-gauges built on GTS-based and historic data, GPCC Data Rep., doi, 10, 2011.

       Sellar, A. A., Jones, C. G., Mulcahy, J., Tang, Y., Yool, A., Wiltshire, A., O'Connor, F. M., Stringer, M., Hill, R., Palmieri, J., Woodward, S.,
       de Mora, L., Kuhlbrodt, T., Rumbold, S., Kelley, D. I., Ellis, R., Johnson, C. E., Walton, J., Abraham, N. L., Andrews, M. B., Andrews,
       T., Archibald, A. T., Berthou, S., Burke, E., Blockley, E., Carslaw, K., Dalvi, M., Edwards, J., Folberth, G. A., Gedney, N., Griffiths,
       P. T., Harper, A. B., Hendry, M. A., Hewitt, A. J., Johnson, B., Jones, A., Jones, C. D., Keeble, J., Liddicoat, S., Morgenstern, O.,
590   Parker, R. J., Predoi, V., Robertson, E., Siahaan, A., Smith, R. S., Swaminathan, R., Woodhouse, M. T., Zeng, G., and Zerroukat, M.:
       UKESM1: Description and evaluation of the UK Earth System Model, Journal of Advances in Modeling Earth Systems, 11, 4513–4558,
       https://doi.org/10.1029/2019MS001739, 2019.

       Seo, J., Choi, W., Youn, D., Park, D.-S. R., and Kim, J. Y.: Relationship between the stratospheric quasi-biennial oscillation and the spring
       rainfall in the western North Pacific, Geophysical Research Letters, 40, 5949–5953, 2013.

595   Serva, F., Cagnazzo, C., Christiansen, B., and Yang, S.: The influence of ENSO events on the stratospheric QBO in a multi-model ensemble,
       Climate Dynamics, 54, 2561–2575, 2020.

       Serva, F., Anstey, J. A., Bushell, A. C., Butchart, N., Cagnazzo, C., Gray, L., Kawatani, Y., Osprey, S. M., Richter, J. H., and Simpson,
       I. R.: The impact of the QBO near the tropical tropopause layer in QBOi models: present-day simulations, Quaterly Journal of the Royal
       Meteorological Society, submitted.

600   Son, S.-W., Lim, Y., Yoo, C., Hendon, H. H., and Kim, J.: Stratospheric control of the Madden–Julian oscillation, Journal of Climate, 30,
       1909–1922, 2017.

Taguchi, M.: Observed connection of the stratospheric quasi-biennial oscillation with El Niño–Southern Oscillation in radiosonde data, Journal of Geophysical Research: Atmospheres, 115, 2010.

Tegtmeier, S., Anstey, J., Davis, S., Ivanciu, I., Jia, Y., McPhee, D., and Pilch Kedzierski, R.: Zonal Asymmetry of the QBO Temperature Signal in the Tropical Tropopause Region, Geophysical Research Letters, 47, e2020GL089 533, https://doi.org/https://doi.org/10.1029/2020GL089533, e2020GL089533 2020GL089533, 2020.

Wang, B. and Ding, Q.: Global monsoon: Dominant mode of annual variation in the tropics, Dynamics of Atmospheres and Oceans, 44, 165–183, 2008.

Wang, B., Biasutti, M., Byrne, M. P., Castro, C., Chang, C.-P., Cook, K., Fu, R., Grimm, A. M., Ha, K.-J., Hendon, H., et al.: Monsoons climate change assessment, Bulletin of the American Meteorological Society, 102, E1–E19, 2021.

Wang, P. X., Wang, B., Cheng, H., Fasullo, J., Guo, Z., Kiefer, T., and Liu, Z.: The global monsoon across time scales: Mechanisms and outstanding issues, Earth-Science Reviews, 174, 84–121, 2017.

Wang, S., Tippett, M. K., Sobel, A. H., Martin, Z., and Vitart, F.: Impact of the QBO on prediction and predictability of the MJO convection, J. Geophys. Res. Atmos, 2019.

Wang, X. and Wang, C.: Different impacts of various El Niño events on the Indian Ocean Dipole, Climate dynamics, 42, 991–1005, 2014.

Williams, K. D., Copsey, D., Blockley, E. W., Bodas-Salcedo, A., Calvert, D., Comer, R., Davis, P., Graham, T., Hewitt, H. T., Hill, R., Hyder, P., Ineson, S., Johns, T. C., Keen, A. B., Lee, R. W., Megann, A., Milton, S. F., Rae, J. G. L., Roberts, M. J., Scaife, A. A., Schiemann, R., Storkey, D., Thorpe, L., Watterson, I. G., Walters, D. N., West, A., Wood, R. A., Woollings, T., and Xavier, P. K.: The Met Office global coupled model 3.0 and 3.1 (GC3. 0 and GC3. 1) configurations, Journal of Advances in Modeling Earth Systems, 10, 357–380, 2018.

Yu, B. and Zwiers, F. W.: Changes in equatorial atmospheric zonal circulations in recent decades, Geophysical Research Letters, 37, 2010.